Acta Crystallographica Section F
Structural Biology and Crystallization Communications
ISSN 1744-3091
Editors: **H. M. Einspahr and M. S. Weiss**

Structure of the recombinant BPTI/Kunitz-type inhibitor *r*ShPI-1A from the marine invertebrate *Stichodactyla helianthus*

Rossana García-Fernández, Tirso Pons, Arne Meyer, Markus Perbandt, Yamile González-González, Dayrom Gil, María de los Angeles Chávez, Christian Betzel and Lars Redecke

Acta Cryst. (2012). F**68**, 1289–1293

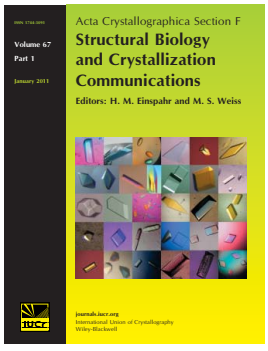

Acta Crystallographica Section F: Structural Biology and Crystallization Communications is a rapid all-electronic journal, which provides a home for short communications on the crystallization and structure of biological macromolecules. Structures determined through structural genomics initiatives or from iterative studies such as those used in the pharmaceutical industry are particularly welcomed. Articles are available online when ready, making publication as fast as possible, and include unlimited free colour illustrations, movies and other enhancements. The editorial process is completely electronic with respect to deposition, submission, refereeing and publication.

Acta Crystallographica Section F
Structural Biology and Crystallization Communications
ISSN 1744-3091

Structure of the recombinant BPTI/Kunitz-type inhibitor *r*ShPI-1A from the marine invertebrate *Stichodactyla helianthus*

Rossana García-Fernández,[a] Tirso Pons,[b] Arne Meyer,[c] Markus Perbandt,[d,e] Yamile González-González,[a] Dayrom Gil,[a] María de los Angeles Chávez,[a] Christian Betzel[d] and Lars Redecke[f]*

[a]Centro de Estudio de Proteínas, Facultad de Biología, Universidad de la Habana, Calle 25 No. 455, Havana 10400, Cuba, [b]Structural Biology and Biocomputing Programme, Spanish National Cancer Research Centre (CNIO), C/Melchor Fernández Almago 3, 28029 Madrid, Spain, [c]Xtal Concepts, Stellinger Steindamm 7, 22527 Hamburg, Germany, [d]Institute of Biochemistry and Molecular Biology, University of Hamburg, c/o DESY, Notkestrasse 85, 22603 Hamburg, Germany, [e]Department of Medical Microbiology, Virology and Hygiene, University Medical Center Hamburg-Eppendorf, Martinistrasse 52, 20246 Hamburg, Germany, and [f]Joint Laboratory for Structural Biology of Infection and Inflammation, Institute of Biochemistry and Molecular Biology, University of Hamburg and Institute of Biochemistry, University of Lübeck, c/o DESY, Notkestrasse 85, 22603 Hamburg, Germany

Correspondence e-mail: redecke@biochem.uni-luebeck.de

Received 3 August 2012
Accepted 12 September 2012

PDB Reference: *r*ShPI-1A, 3ofw

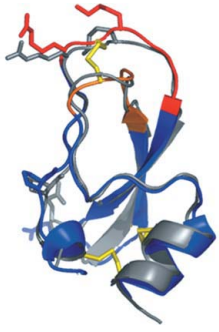

The BPTI/Kunitz-type inhibitor family includes several extremely potent serine protease inhibitors. To date, the inhibitory mechanisms have only been studied for mammalian inhibitors. Here, the first crystal structure of a BPTI/Kunitz-type inhibitor from a marine invertebrate (*r*ShPI-1A) is reported to 2.5 Å resolution. Crystallization of recombinant *r*ShPI-1A required the salt-induced dissociation of a trypsin complex that was previously formed to avoid intrinsic inhibitor aggregates in solution. The *r*ShPI-1A structure is similar to the NMR structure of the molecule purified from the natural source, but allowed the assignment of disulfide-bridge chiralities and the detection of an internal stabilizing water network. A structural comparison with other BPTI/Kunitz-type canonical inhibitors revealed unusual φ angles at positions 17 and 30 to be a particular characteristic of the family. A significant clustering of φ and ψ angle values in the glycine-rich remote fragment near the secondary binding loop was additionally identified, but its impact on the specificity of *r*ShPI-1A and similar molecules requires further study.

1. Introduction

The BPTI/Kunitz-type inhibitor family (Pfam PF00014; Finn *et al.*, 2010) includes some of the most extensively studied canonical serine protease inhibitors, which have been isolated from invertebrate to mammalian species (Laskowski *et al.*, 2000; Kunitz & Northrop, 1936; Delfín *et al.*, 1996). Canonical BPTI/Kunitz-type inhibitors are small protein domains (of around 6 kDa) with a compact hydrophobic core structure containing a central β-sheet and three conserved disulfide bridges (Antuch *et al.*, 1993; Scheidig *et al.*, 1997; Czapinska *et al.*, 2000). The extreme stability of the target enzyme interaction, which is characterized by dissociation constants ranging from 10^{-13} to 10^{-7} *M*, results from a substrate-like interaction of the convex exposed binding loop with the highly complementary concave protease active site (Laskowski *et al.*, 2000). The association energy depends mainly on the residue at position P1, supported by further residues within the primary binding site and the secondary binding loop of the inhibitor (Scheidig *et al.*, 1997; Laskowski *et al.*, 2000; Czapinska *et al.*, 2000). The majority of the structures that have been determined to study the inhibitory activity are of bovine pancreatic trypsin inhibitor (BPTI; Huber *et al.*, 1974; Burgering *et al.*, 1997; Scheidig *et al.*, 1997). We have previously reported the isolation of ShPI-1, a protease inhibitor from the Caribbean sea anemone *Stichodactyla helianthus* that shares the common structure of the BPTI/Kunitz-type family (PDB entry 1shp; Antuch *et al.*, 1993) but exhibits an unusually broad specificity (Delfín *et al.*, 1996). The recent high-level expression of a recombinant variant of ShPI-1 (*r*ShPI-1A; Gil *et al.*, 2011) enabled its structural investigation by X-ray crystallography. Although the *r*ShPI-1A structure closely resembles the previously determined NMR structure of ShPI-1 purified from the natural source (PDB entry 1shp; Antuch *et al.*, 1993), an internal water-stabilization network as well as the disulfide-bridge chiralities were revealed that had not previously been identified, thereby extending the structural characterization of this multifunctional invertebrate inhibitor.

Table 1
Protein-production information.

Source organism	*S. helianthus* strain KM71H
Expression vector	pZErO-2.1
Expression host	*Pichia pastoris*
Complete amino-acid sequence of the construct produced	EAEASICSEPKKVGRCKGYFPRFYFDSETGKC-TPFIYGGCGGNGNNFETLHQCRAICRALG

Table 2
Data-collection and processing statistics.

Values in parentheses are for the outer shell.

Diffraction source	Rigaku RU-200 rotating anode
Wavelength (Å)	1.5418
Temperature (K)	293
Detector	180 mm MAR Research image plate
Crystal-to-detector distance (mm)	120
Rotation range per image (°)	1.5
Total rotation range (°)	129
Exposure time per image (s)	240
Space group	$P4_32_12$
Unit-cell parameters (Å)	$a = b = 37.16$, $c = 114.98$
Mosaicity (°)	0.48
Resolution range (Å)	35.36–2.50 (2.64–2.50)
Total No. of reflections	15197
No. of unique reflections	3127
Completeness (%)	99.0 (100)
Multiplicity	4.9 (5.0)
$\langle I/\sigma(I)\rangle$	5.8 (3.1)
$R_{\rm r.i.m.}$†	0.111 (0.235)
Overall *B* factor from Wilson plot (Å^2)	30.2

† Estimated $R_{\rm r.i.m.} = R_{\rm merge}[N/(N-1)]^{1/2}$, where N is the data multiplicity.

2. Materials and methods

2.1. Protein production

Recombinant *r*ShPI-1A was expressed and purified as described by Gil *et al.* (2011) (Table 1). The product includes additional residues at the N-terminus (Glu−3, Ala−2, Glu−1 and Ala0) and at the C-terminus (Leu56 and Gly57). Two different approaches for concentration of *r*ShPI-1A buffered in 20 m*M* Tris–HCl pH 8.0, 1.0 *M* NaCl (buffer 1) were tested: lyophilization and re-solution in water (solution *A*) and concentration by ultrafiltration (solution *B*) using Centricon CM-3 concentration devices (Millipore). Protein concentration was determined from the absorbance at 280 nm ($\varepsilon^{0.1\%}_{280\ \rm nm} = 0.52$). Activity was confirmed by inhibition of bovine pancreatic trypsin (EC 3.4.21.4; Sigma) as described by Erlanger *et al.* (1961). Far-UV (190–260 nm) circular-dichroism (CD) spectroscopy and dynamic light-scattering (DLS) measurements were performed as described by Redecke *et al.* (2009) using a J-715 spectropolarimeter (Jasco) and a Spectroscatterer 201 (Molecular Dimensions), respectively. Molecular masses were calculated from hydrodynamic radii using *SpectroSize* (Fischer *et al.*, 2004). The theoretical $R_{\rm h}$ of natural ShPI-1 was estimated from its monomeric NMR structure (Antuch *et al.*, 1993) using *HYDROPRO* (García de la Torre *et al.*, 2000).

2.2. Crystallization

Hanging-drop vapour-diffusion crystallization trials (1 µl protein solution in buffer 1 plus 1 µl reservoir solution equilibrated against 500 µl reservoir solution) were performed with *r*ShPI-1A solutions *A* (4.0 m*M*) and *B* (3.5 m*M*) applying the reservoir buffer conditions previously reported for the crystallization of homologous BPTI/Kunitz-type domains in the Biological Macromolecule Crystallization Database (BMCD; Tung & Gallagher, 2009). In addition, binary complexes formed after incubation of *r*ShPI-1A solutions *A* and *B* with equimolar concentrations of bovine pancreatic trypsin (EC 3.4.21.4; Sigma) for 1 h at 298 K were screened for crystal growth applying identical conditions as used for the free inhibitors. Crystals measuring up to 0.4 mm in size grew within one week at 288 K only in setups containing trypsin complexes of *r*ShPI-1A sample *A* or *B* with a reservoir solution consisting of 0.1 *M* Tris–HCl pH 8.5, 1.7 *M* ammonium sulfate, 6%(*w*/*v*) glycerol. No crystallization conditions were identified for uncomplexed inhibitor solutions *A* and *B*.

2.3. Data collection and processing

A single protein crystal grown in a setup containing the binary trypsin complex formed using *r*ShPI-1A solution *A* was mounted in a capillary. Diffraction data were collected at 293 K to 2.5 Å resolution using an in-house Rigaku RU-200 rotating-anode X-ray generator operated at 50 kV and 100 mA and equipped with a MAR Research image-plate detector. Data were reduced using *MOSFLM* (Leslie & Powell, 2007) and *SCALA* (Winn *et al.*, 2011). Full details are presented in Table 2.

2.4. Structure solution and refinement

The structure was solved by molecular replacement with *MOLREP* (Winn *et al.*, 2011) using the NMR coordinates of natural ShPI-1 (Antuch *et al.*, 1993; PDB entry 1shp) as a search model. The structure was refined with *REFMAC* v.5.2.0019 (Murshudov *et al.*, 2011) and by manual intervention employing *Coot* (Emsley *et al.*, 2010). The electron density was well defined by the *r*ShPI-1A model, but features corresponding to a bound trypsin molecule were not detected. Furthermore, the Matthews coefficient of 3.27 Å^3 Da^{-1} (Matthews, 1968) corroborated the presence of one *r*ShPI-1A molecule in the asymmetric unit. *MolProbity* (Chen *et al.*, 2010) was

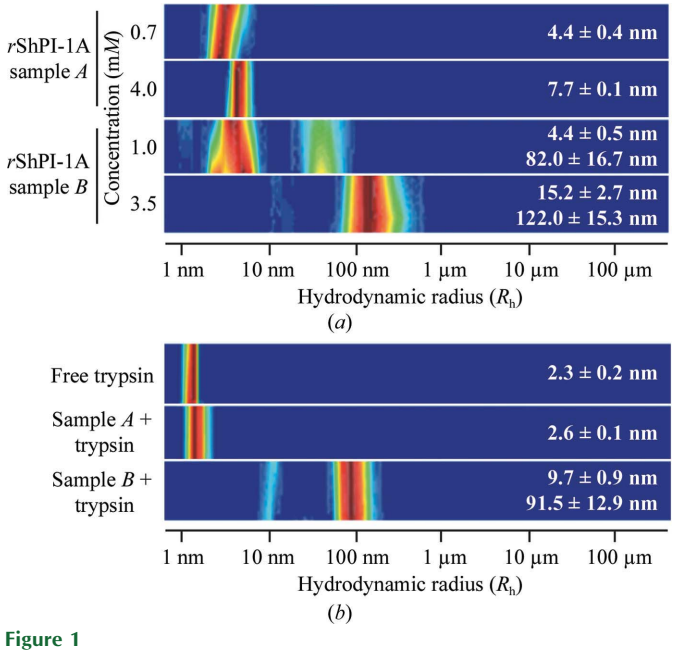

Figure 1
(*a*) DLS analysis of the *r*ShPI-1A aggregation state in solution after concentration by different techniques. Lyophilization (sample *A*) induced *r*ShPI-1A oligomerization, while large inhomogeneous aggregates are formed by ultrafiltration (sample *B*). For monomeric ShPI-1 a theoretical hydrodynamic radius ($R_{\rm h}$) of 1.6 nm was calculated. (*b*) In the presence of equimolar concentrations of trypsin, *r*ShPI-1A disaggregates in solution *A* (4.0 m*M*) owing to complex formation, while the heterogeneous radius distribution in solution *B* (3.5 m*M*) is not affected. DLS analysis of free trypsin is shown for comparison. The colour code corresponds to the relative frequency of particles characterized by a specific radius in solution, with dark red being the highest and blue the lowest.

used for structure validation and Ramachandran analysis. Asn41 and Asn44 were outside the allowed regions of the Ramachandran plot, but were well defined in the electron-density map. The equivalent residues exhibited less favourable φ/ψ angles in all known structures of BPTI (Czapinska *et al.*, 2000). No further geometric conflicts were detected. Refinement statistics are summarized in Table 3. Calculations of the torsion angles, the intramolecular hydrogen bonds and of the average NMR structure of natural ShPI-1 as well as the structural alignment with 12 BPTI/Kunitz-type domains were performed with *WHAT IF* (Vriend, 1990).

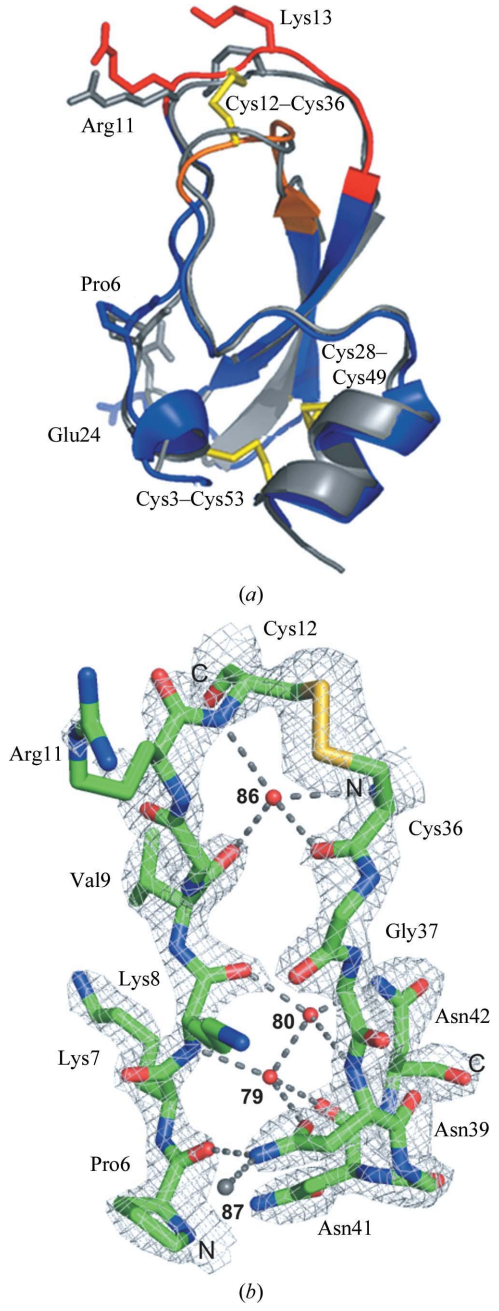

Figure 2
(*a*) Superposition of the three-dimensional structure of free *r*ShPI-1A (blue) and the average NMR structure of ShPI-1 purified from the natural source (grey). The canonical (P3–P3′) and secondary (Ile32–Gly37) binding loops are highlighted in red and orange, respectively, while the conserved disulfide bridges are shown in yellow stick representation. Residues with backbone r.m.s.d.s of more than 1.7 Å are labelled. (*b*) Internal water-coordination sites near the binding loops of *r*ShPI-1A. The shifted water molecule (87) observed in *r*ShPI-1A is shown in grey. Dashed lines represent water-mediated hydrogen bonds. The unusual right-handed conformation of the Cys12–Cys36 disulfide bridge is well defined by the electron density (grey mesh, 2σ).

Table 3
Structure refinement.

Values in parentheses are for the outer shell.

Resolution range (Å)	28.80–2.50 (2.57–2.50)
Completeness (%)	98.4
σ cutoff	None
No. of reflections, working set	2955 (210)
No. of reflections, test set	135 (6)
Final R_{cryst}	0.190 (0.258)
Final R_{free}	0.221 (0.373)
No. of non-H atoms	
Protein	444
Ions (Cl^-)	3
Waters	28
Total	475
R.m.s. deviations	
Bonds (Å)	0.012
Angles (°)	1.402
Average *B* factors (Å^2)	
Protein	21.4
Ions (Cl^-)	46.0
Waters	28.0
Ramachandran plot (%)	
Favoured regions	94.7
Additionally allowed	3.5
Outliers	1.8

3. Results and discussion

Depending on the protein concentration and on the concentration technique applied, purified *r*ShPI-1A aggregates in solution (Fig. 1*a*). Nonspecific self-association during ultrafiltration has previously been attributed to mechanical stress on the protein at the membrane surface (Cromwell *et al.*, 2006). A locally high protein concentration compared with the bulk solution favours concentration-dependent aggregation. During lyophilization, however, the ionic strength increases with the reduced volume of the solution, which is suggested to prevent the formation of large *r*ShPI-1A aggregates, as observed for BPTI (Lafont *et al.*, 1994). Neither the freezing process during lyophilization nor the aggregation state affected the native secondary structure of the inhibitor, as shown by the almost identical far-UV CD spectra obtained for both samples, which displayed the curve progression expected for *r*ShPI-1A (Gil *et al.*, 2011; Supplementary Fig. S1[1]). Oligomeric *r*ShPI-1A in the lyophilized sample (sample *A*) disassembled on complex formation with trypsin into monomeric enzyme–inhibitor complexes, while the ultrafiltered sample B remained highly heterogeneous (Fig. 1*b*). Crystals grown using the monomeric complex setup appeared to be optimized regarding size and quality by visual inspection (Supplementary Fig. S2[1]). Thus, a single crystal from this setup was used for diffraction data collection. Interestingly, the asymmetric unit contained only free *r*ShPI-1A, not the expected inhibitor–trypsin complex, suggesting that crystallization was a consequence of salt-induced complex dissociation induced by the precipitant solution. A comparable crystallization chaperone effect has been reported for other canonical serine protease inhibitors, *e.g.* eglin C in the presence of subtilisin DY (Betzel *et al.*, 1993), but has not been reported to date for the crystallization of canonical BPTI/Kunitz-type inhibitors. The X-ray structure of *r*ShPI-1A (Fig. 2*a*) is highly similar to the NMR structure of the molecule purified from the natural source (average backbone

[1] Supplementary material has been deposited in the IUCr electronic archive (Reference: EN5515).

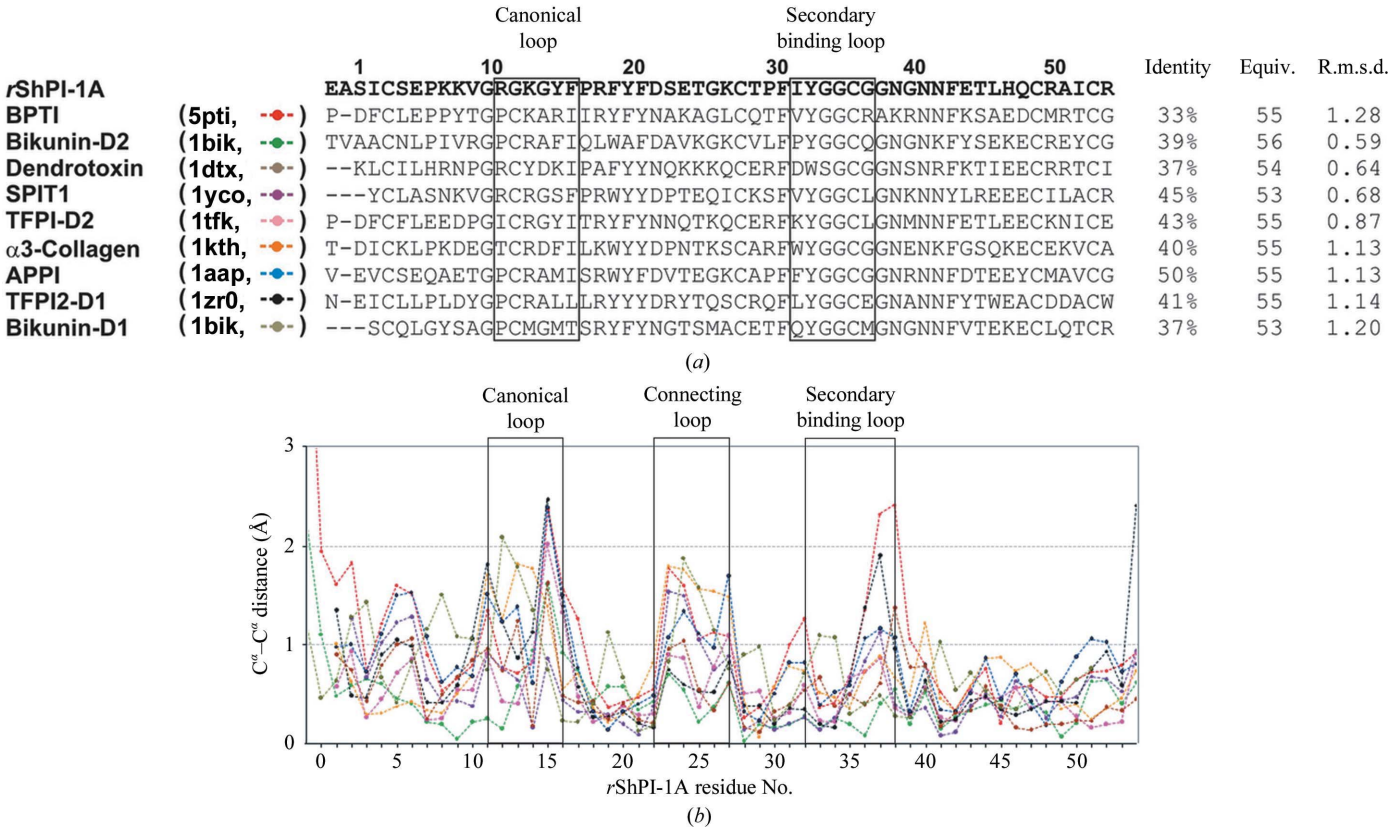

Figure 3
(*a*) Structure-based multiple sequence alignment of BPTI/Kunitz-type canonical domains. The domain names and the PDB codes are shown on the left, while the sequence identity (%), the number of equivalent/total compared C^{α} atoms and the resulting r.m.s.d. values are displayed on the right. The canonical (P3–P3′) and secondary binding loops (residues 32–37 in *r*ShPI-1A) are highlighted in boxes. (*b*) C^{α} deviations (Å) of the analyzed BPTI/Kunitz-type canonical domains compared with *r*ShPI-1A (from Ala0 to Arg54 in *r*ShPI-1A numbering). Line identifiers correspond to the associated sequences of the BPTI/Kunitz-type domains shown in (*a*).

r.m.s.d. 0.89 Å; Antuch *et al.*, 1993). Thus, the native fold was not affected by the additional residues at the N- and C-termini. Backbone r.m.s.d.s of more than 1.7 Å are restricted to residues Pro6, Arg11, Lys13 and Glu24. The increased *B* factors of Pro6 and Glu24 reflect the enhanced flexibility of the N-terminal residues and of the small loop connecting the two β-strands where these residues are located. In contrast, the deviations of Arg11 and Lys13 are attributed to the involvement of both residues in strong crystal contacts which reduce the overall flexibility of the canonical loop in the crystal structure compared with the NMR model, as indicated by the low *B* factors. A preferred left-handed conformation was assigned to the disulfide bridges Cys3–Cys53 and Cys28–Cys49, while Cys12–Cys36 adopts the unusual right-handed conformation (Fig. 2*a*) common in BPTI/Kunitz-type inhibitors (Czapinska *et al.*, 2000). The coexistence of both chiralities at Cys12–Cys36 previously observed in BPTI structures was not detected (Otting *et al.*, 1993; Czapinska *et al.*, 2000). The impact of disulfide-bond chiralities on the conformation and the flexibility of the binding loop in BPTI/Kunitz-type domains is still under discussion (Petersen *et al.*, 1996; Czapinska *et al.*, 2000). *r*ShPI-1A is stabilized by an internal network of only three buried water molecules, which are located in a tetrahedral coordination highly similar to those in BPTI (Fig. 2*b*; Deisenhofer & Steigemann, 1975; Wlodawer *et al.*, 1984). The fourth internal water molecule is present, but is shifted by the side chain of Asn39 into a slightly different position compared with that in BPTI, preventing a contribution to the network. However, the overall *r*ShPI-1A stability is compensated by a direct interaction between Pro6 and Asn39.

Comparison of *r*ShPI-1A with all crystal structures of BPTI/Kunitz-type canonical domains currently annotated in the PDB (Fig. 3*a*) confirms the structural conservation, including the intramolecular hydrogen-bond network. Significant C^{α} deviations (>1 Å) are restricted to flexible loop regions (Fig. 3*b*). φ angles unusual for β-sheet structures at the nonconserved residues Pro17 and Pro30 of ShPI-1 have previously been associated with its reduced thermostability compared with BPTI (Antuch *et al.*, 1993). However, we identified unusual φ angles at the equivalent positions in all canonical BPTI/Kunitz-type domains independent of the residue that was present (Supplementary Fig. S3*a*). Thus, a contribution of this characteristic feature of canonical BPTI/Kunitz-type inhibitors to the structural restraints for the highly twisted antiparallel β-sheet is more likely than a correlation with the different stability of these inhibitors, which requires further investigation. Moreover, a specific φ/ψ-angle clustering was detected for equivalent residues that compose the glycine-rich remote fragment (Supplementary Figs. S3*b* and S3*c*), which has been linked to the specificity and binding affinity of BPTI/Kunitz-type domains by restricting the available inhibitor conformations (Pritchard & Dufton, 1999). However, further studies are required in order to investigate the contribution of this region to the broad specificity of ShPI-1, which has previously been associated with a defensive role in *S. helianthus* (Delfín *et al.*, 1996).

This work was partially supported by the International Foundation for Science (IFS), Sweden (grant F4086) and the Deutscher Akade-

mischer Austausch Dienst (DAAD). CB and LR thank the German Federal Ministry of Education and Research (BMBF) for financial support (grants 01KX0806 and 01KX0807). We are indebted to Professor Dr Hahn for his support in starting this research and Professor Dr J. Díaz and Dr M. Mansur for their contributions to the heterologous expression of *r*ShPI-1A. We acknowledge Dr T. Bergfors (Biomedical Center, Uppsala University, Sweden) for helpful advice during the crystallization experiments.

References

Antuch, W., Berndt, K. D., Chávez, M. A., Delfín, J. & Wüthrich, K. (1993). *Eur. J. Biochem.* **212**, 675–684.
Betzel, C., Dauter, Z., Genov, N., Lamzin, V., Navaza, J., Schnebli, H. P., Visanji, M. & Wilson, K. S. (1993). *FEBS Lett.* **317**, 185–188.
Burgering, M. J., Orbons, L. P., van der Doelen, A., Mulders, J., Theunissen, H. J., Grootenhuis, P. D., Bode, W., Huber, R. & Stubbs, M. T. (1997). *J. Mol. Biol.* **269**, 395–407.
Chen, V. B., Arendall, W. B., Headd, J. J., Keedy, D. A., Immormino, R. M., Kapral, G. J., Murray, L. W., Richardson, J. S. & Richardson, D. C. (2010). *Acta Cryst.* D**66**, 12–21.
Cromwell, M. E. M., Hilario, E. & Jacobson, F. (2006). *AAPS J.* **8**, E572–E579.
Czapinska, H., Otlewski, J., Krzywda, S., Sheldrick, G. M. & Jaskólski, M. (2000). *J. Mol. Biol.* **295**, 1237–1249.
Deisenhofer, J. & Steigemann, W. (1975). *Acta Cryst.* B**31**, 238–250.
Delfín, J., Martínez, I., Antuch, W., Morera, V., González, Y., Rodríguez, R., Márquez, M., Saroyán, A., Larionova, N., Díaz, J., Padrón, G. & Chávez, M. (1996). *Toxicon*, **34**, 1367–1376.
Emsley, P., Lohkamp, B., Scott, W. G. & Cowtan, K. (2010). *Acta Cryst.* D**66**, 486–501.
Erlanger, B. F., Kokowsky, N. & Cohen, W. (1961). *Arch. Biochem. Biophys.* **95**, 271–278.
Finn, R. D., Mistry, J., Tate, J., Coggill, P., Heger, A., Pollington, J. E., Gavin, O. L., Gunasekaran, P., Ceric, G., Forslund, K., Holm, L., Sonnhammer, E. L., Eddy, S. R. & Bateman, A. (2010). *Nucleic Acids Res.* **38**, D211–D222.
Fischer, H., Polikarpov, I. & Craievich, A. F. (2004). *Protein Sci.* **13**, 2825–2828.
García De La Torre, J., Huertas, M. L. & Carrasco, B. (2000). *Biophys. J.* **78**, 719–730.
Gil, D. F., García-Fernández, R., Alonso-del-Rivero, M., Lamazares, E., Pérez, M., Varas, L., Díaz, J., Chávez, M. A., González-González, Y. & Mansur, M. (2011). *FEMS Yeast Res.* **11**, 575–586.
Huber, R., Kukla, D., Bode, W., Schwager, P., Bartels, K., Deisenhofer, J. & Steigemann, W. (1974). *J. Mol. Biol.* **89**, 73–101.
Kunitz, M. & Northrop, J. H. (1936). *J. Gen. Physiol.* **19**, 991–1007.
Lafont, S., Veesler, S., Astier, J. P. & Boistelle, R. (1994). *J. Cryst. Growth*, **143**, 249–255.
Laskowski, M. Jr, Qasim, M. A. & Lu, S. M. (2000). *Protein–Protein Recognition*, edited by C. Kleanthous, pp. 228–279. Oxford University Press.
Leslie, A. G. W. & Powell, H. R. (2007). *Evolving Methods for Macromolecular Crystallography*, edited by R. J. Read & J. L. Sussman, pp. 41–51. Dordrecht: Springer.
Matthews, B. W. (1968). *J. Mol. Biol.* **33**, 491–497.
Murshudov, G. N., Skubák, P., Lebedev, A. A., Pannu, N. S., Steiner, R. A., Nicholls, R. A., Winn, M. D., Long, F. & Vagin, A. A. (2011). *Acta Cryst.* D**67**, 355–367.
Otting, G., Liepinsh, E. & Wüthrich, K. (1993). *Biochemistry*, **32**, 3571–3582.
Petersen, L. C., Bjørn, S. E., Olsen, O. H., Nordfang, O., Norris, F. & Norris, K. (1996). *Eur. J. Biochem.* **235**, 310–316.
Pritchard, L. & Dufton, M. J. (1999). *J. Mol. Biol.* **285**, 1589–1607.
Redecke, L., Binder, S., Elmallah, M. I., Broadbent, R., Tilkorn, C., Schulz, B., May, P., Goos, A., Eich, A., Rübhausen, M. & Betzel, C. (2009). *Free Radic. Biol. Med.* **46**, 1353–1361.
Scheidig, A. J., Hynes, T. R., Pelletier, L. A., Wells, J. A. & Kossiakoff, A. A. (1997). *Protein Sci.* **6**, 1806–1824.
Tung, M. & Gallagher, D. T. (2009). *Acta Cryst.* D**65**, 18–23.
Vriend, G. (1990). *J. Mol. Graph.* **8**, 52–56.
Winn, M. D. *et al.* (2011). *Acta Cryst.* D**67**, 235–242.
Wlodawer, A., Walter, J., Huber, R. & Sjölin, L. (1984). *J. Mol. Biol.* **180**, 301–329.